BIOLOGICAL SCIENCES: Microbiology

A specific non-bisphosphonate inhibitor of the bifunctional farnesyl/geranylgeranyl diphosphate synthase in malaria parasites

Jolyn E. Gisselberg[1], Zachary Herrera[1], Lindsey Orchard[4], Manuel Llinás[4,5,6], and Ellen Yeh[1,2,3*]

[1]Department of Biochemistry, [2]Pathology, and [3]Microbiology and Immunology, Stanford Medical School, Stanford University, Stanford, CA 94025, USA

[4]Department of Biochemistry & Molecular Biology, [5]Department of Chemistry and [6]Huck Center for Malaria Research, Pennsylvania State University, University Park, PA 16802

*Corresponding author: ellenyeh@stanford.edu

Keywords: malaria, drug discovery, and high-throughput screening, non-bisphosphonate inhibitor

Abstract

There are multiple validated antimalarial drug targets in isoprenoid biosynthetic pathways. Using a growth rescue screen, we identified MMV019313 as an inhibitor of isoprenoid biosynthesis in *Plasmodium falciparum* parasites that cause malaria. We demonstrate that the molecular target of MMV019313 is the *P. falciparum* bifunctional farnesyl and geranylgeranyl diphosphate synthase (FPPS/GGPPS): Both an S228T variant and overexpression of wildtype *Pf*FPPS/GGPPS conferred resistance to MMV019313. MMV019313 also inhibited the activity of purified *Pf*FPPS/GGPPS. *Pf*FPPS/GGPPS has already been validated as an antimalarial drug target since its inhibition by bisphosphonates, a class of drugs that inhibits human FPPS, was shown to clear parasitemia in a mouse malaria model. Though bisphosphonates are clinically used for treating osteoporosis, MMV019313 has significant advantages over bisphosphonates for antimalarial drug development. MMV019313 has superior physicochemical properties compared to charged bisphosphonates that have poor bioavailability and strong bone affinity. We also show that it is highly selective for *Pf*FPPS/GGPPS and showed no activity against human FPPS or GGPPS. Inhibition of *Pf*FPPS/GGPPS by MMV019313, but not bisphosphonates, was disrupted in the S228T variant, demonstrating that MMV019313 and bisphosphonates have distinct modes-of-inhibition against *Pf*FPPS/GGPPS. In addition, we describe two methodological improvements: a more sensitive chemical rescue screen for identifying isoprenoid inhibitors and the first report using chemical mutagenesis for drug resistance selection in *Plasmodium*. Altogether MMV019313 is the first specific, non-bisphosphonate inhibitor of *Pf*FPPS/GGPPS. Our findings uncover a new small molecule binding site in this important antimalarial drug target and provide a promising starting point for development of *Plasmodium*-specific FPPS/GGPPS inhibitors.

Significance Statement

There is an urgent need for antimalarials with novel mechanisms-of-action to circumvent resistance to frontline drugs. Isoprenoid biosynthetic pathways are essential for *Plasmodium* (malaria) parasites and contain multiple validated drug targets. We identify a new antimalarial compound that inhibits a key branchpoint enzyme in isoprenoid biosynthesis. Our compound has significant advantages over bisphosphonate inhibitors that inhibit the same drug target with improved drug properties and specificity for the *Plasmodium* enzyme over human homologs. Our findings uncover a new "druggable" site in this important antimalarial drug target and provide a chemical starting point for development of *Plasmodium*-specific FPPS/GGPPS inhibitors.

Introduction

There is an urgent need for antimalarials with novel mechanisms-of-action to circumvent resistance to frontline drugs. The biosynthesis of cellular isoprenoids is an essential process in *Plasmodium* parasites that cause malaria. A number of antimalarial compounds target enzymes in isoprenoid biosynthetic pathways leading to parasite growth inhibition. First, *Plasmodium* parasites depend on the 7-enzyme prokaryotic 2-*C*-methyl-D-erythritol 4-phosphate (MEP) pathway in its plastid organelle, the apicoplast, to produce isopentenyl pyrophosphate (IPP) and its isomer dimethyallyl pyrophosphate (DMAPP) (1). IPP and DMAPP are the C5 building blocks for all isoprenoids. The antibiotic fosmidomycin inhibits the MEP enzyme, Dxr/IspC, in both bacteria and *Plasmodium* parasites (1).

Second, at least three isoprenoid synthases (PF3D7_1128400.1, PF3D7_0202700, PF3D7_0826400) catalyze the condensation of IPP and DMAPP into longer prenyl chains (2-4).

In particular, farnesyl pyrophosphate synthase (FPPS) and geranylgeranyl pyrophosphate synthase (GGPPS) are key branch point enzymes that synthesize C15 and C20 prenyl chains, respectively, for multiple downstream enzymes. Nitrogen-containing bisphosphonates, blockbuster drugs which inhibit human FPPS, also inhibit the bifunctional FPPS/GGPPS found in *Plasmodium* parasites (5-9).

Finally, prenyl chains are cyclized and/or conjugated to small molecule and protein scaffolds by a variety of prenyltransferases to biosynthesize final isoprenoid products required for parasite growth and replication. Tetrahydroquinolines (THQ) have been shown to potently inhibit the *Plasmodium* protein farnesyltransferase (10-12). Other inhibitors may interfere with isoprenoid biosynthesis indirectly by disrupting transporters that supply starting substrates or export products or blocking pathways that provide cofactors for isoprenoid biosynthetic enzymes.

Importantly fosmidomycin, bisphosphonates, and tetrahydroquinolines have all shown efficacy in mouse models of malaria infection, validating the key importance of isoprenoid biosynthesis as an antimalarial drug target (1, 5, 6, 10). Fosmidomycin is currently being tested in human clinical trials, while a THQ lead candidate was investigated in preclinical studies (10, 13). However, novel chemical scaffolds that disrupt isoprenoid biosynthetic pathways in *Plasmodium* remain desirable to overcome unfavorable drug properties of these known inhibitors. For example, bisphosphonates avidly bind bone mineral, and both fosmidomycin and THQs have short half-lives *in vivo* (14-16).

In 2011 the Medicine for Malaria Venture (MMV) distributed the Open-Access Malaria Box to accelerate antimalarial drug discovery (17). The Malaria Box consists of 400 structurally diverse compounds, curated from >20,000 hits generated from large-scale screens, that inhibit the growth of blood-stage *Plasmodium falciparum* parasites (18-20). A major goal of sharing these compounds was to facilitate elucidation of their antimalarial mechanism-of-action and open new classes of validated chemical scaffolds and drug targets. Compounds that disrupt isoprenoid metabolism can be detected by "rescue" of their growth inhibition upon supplementation of isoprenoids in the growth media (21). Previously, we and two other groups screened the Malaria Box for compounds whose growth inhibition were rescued by addition of IPP and identified MMV008138 (22, 23). We and our collaborators demonstrated that MMV008138 inhibits IspD, an enzyme in the MEP pathway that produces IPP (23).

Using a quantitative high-throughput screen (qHTS), we report a second compound in the Malaria Box, MMV019313, that shows an IPP rescue phenotype but was not identified in screens performed by other groups (22, 24, 25). We demonstrate that the target of MMV019313 is the *P. falciparum* FPPS/GGPPS, a cytosolic isoprenoid synthase that utilizes IPP and the key branch point enzyme in isoprenoid biosynthesis in parasites. MMV019313 represents the first new class of non-bisphosphonate inhibitors of *Pf*FPPS/GGPPS.

Results

A quantitative high-throughput screen (qHTS) for growth and IPP rescue identifies MMV019313 as an inhibitor of isoprenoid biosynthesis

Previous IPP rescue screens of the Malaria Box tested compounds at a single, high concentration >5 μM (22, 24, 25). While testing compounds at a single concentration is useful for identifying phenotypes that occur at a threshold concentration (e.g. growth inhibition), growth rescue is expected to occur within a specific range of concentrations. For example,

110 doxycycline inhibits *P. falciparum* growth with an EC_{50}= 0.3 μM that increases to 3.2 μM upon
111 addition of IPP (21). At concentrations <0.3 μM, doxycycline does not cause growth inhibition.
112 However, at concentrations >3.2 μM, it is no longer specific for its target and causes growth
113 inhibition through additional targets that cannot be IPP rescued. Therefore the concentration
114 range in which IPP rescue can be observed is greater than the EC_{50} of the compound for its
115 specific, IPP-rescuable target but less than that for any nonspecific targets.
116 To increase the sensitivity for detecting IPP chemical rescue, we screened the Malaria
117 Box for growth inhibition of blood-stage *P. falciparum* in the presence and absence of IPP over
118 8-12 drug concentrations from 0.01-27 μM (Table S1). Of 397 compounds tested (3 compounds
119 were not available), 383 showed growth inhibition at ≤27 μM. Initial hits showing IPP rescue of
120 growth inhibition at one or more drug concentrations were commercially sourced and retested.
121 Along with the previously reported compound, MMV008138, we confirmed a second compound
122 in the Malaria Box showing an IPP rescue phenotype, MMV019313 (Figure 1A). MMV019313
123 inhibited *P. falciparum* growth measured in a single replication cycle with EC_{50}=268 nM (250-
124 289 nM) in the absence of IPP; in the presence of IPP, the EC_{50} was over 13-fold more at 3.6 μM
125 (3.2-4.0 μM) (Figure 1B). Notably, at concentrations >3.6 μM, MMV019313 inhibits a
126 nonspecific target that can no longer be IPP rescued, which explains why it was not identified in
127 previous screens.
128 An unusual feature of blood-stage *Plasmodium* is that IPP can rescue complete loss of the
129 apicoplast, the plastid organelle which houses the MEP pathway, since production of IPP is the
130 only essential function of the apicoplast. Compounds like doxycycline that disrupt apicoplast
131 biogenesis cause growth inhibition rescued by IPP and result in parasites lacking an apicoplast
132 (21). In contrast, inhibitors of isoprenoid biosynthesis, like fosmidomycin and MMV008138,
133 cause growth inhibition rescued by IPP with an intact apicoplast (26). We determined whether
134 MMV019313 disrupted the biogenesis of the apicoplast. Both the replication of the apicoplast
135 genome and import of an apicoplast-targeted GFP were intact in MMV019313-treated and IPP-
136 rescued parasites (Figure S1; 21). Altogether MMV019313 causes growth inhibition rescued by
137 IPP with no defect in apicoplast biogenesis, suggesting that, like fosmidomycin and
138 MMV008138, MMV019313 blocks isoprenoid biosynthesis (23).
139
140 **MMV019313-resistant parasites contain a mutation in the geranylgeranyl diphosphate**
141 **synthase**
142 To gain further insight into the mechanism-of-action of MMV019313, we identified
143 mutations that confer resistance to MMV019313. Our initial attempt to select drug-resistant
144 parasites from a bulk culture of 10^{10} parasites was not successful, though this same protocol was
145 effective in selecting drug resistance against MMV008138 when performed in parallel (23).
146 Therefore, we turned to chemical mutagenesis to increase the likelihood of selecting
147 MMV019313-resistant parasites. Chemical mutagenesis has been successfully employed to
148 perform genetic screens in *T. gondii* but, to our knowledge, has not been used in *Plasmodium*
149 parasites (27). We treated 10^8 *P. falciparum* W2 parasites with sub-lethal doses of ethyl
150 methanesulfonate (EMS), an alkylating agent. Because EMS is unstable, we tested a fresh batch
151 of mutagen immediately prior to treatment in a standard parasite growth inhibition assay to
152 determine its EC_{50}. We then selected the EC_{50} as the highest mutagen concentration used and
153 also tested several lower concentrations by serially diluting 3-fold. These concentrations were
154 selected to maximize the frequency of drug-resistant mutations while minimizing lethal
155 mutations that would result in a smaller pool of starting parasites or nonspecific passenger

156 mutations that would confound identification of causative mutations. Following mutagenesis,
157 parasites were continuously selected with a dose of MMV019313 equal to its EC_{75} in the
158 presence of IPP for 7 or 32 days before removal of the drug. This concentration was chosen to
159 maximize selection pressure for developing resistance in the IPP-rescuable target, while
160 minimizing that for developing resistance in nonspecific targets.
161 Resistant parasites emerged in all mutagenized cultures one week after drug removal. In
162 these resistant populations, MMV019313 showed EC_{50} values that ranged from 3-9-fold greater
163 than that observed in the initial susceptible population. Growth inhibition of two MMV019313-
164 resistant populations which showed the highest levels of resistance at the lowest EMS
165 concentrations used, designated 019313R1 and 019313R2, are shown in Figure 2A. Significantly
166 the EC_{50} of MMV019313 in 019313R1 and 019313R2 was similar to that observed in susceptible
167 strains in the presence of IPP, and growth inhibition could no longer be rescued by addition of
168 IPP (Figure S2). These results suggest that, as expected, 019313R1 and 019313R2 populations
169 were completely resistant to inhibition of its specific IPP-rescuable target but had not developed
170 resistance to inhibition of additional nonspecific targets. This is the first example of using
171 chemical mutagenesis to aid selection of drug-resistant parasites in *P. falciparum.*
172 019313R1, 019313R2, and their respective mutagenized parent strains used to initiate
173 drug selection, WT1 and WT2, were subjected to whole-genome sequencing. Comparison of the
174 resistant and parent genome sequences identified a single nucleotide variant (SNV) which was
175 present in 100% of reads in 019313R1 and 63% of reads in 019313R2 but not present in either
176 susceptible parent genomes (Table 1). No other SNV were detected at >40% prevalence in either
177 resistant populations relative to the corresponding parent populations. The identified SNV was a
178 T-to-A mutation in the gene PF3D7_1128400 characterized as a bifunctional FPPS/GGPPS and
179 resulted in a Ser228-to-Thr change in the protein (Figure 2B; 2, 4). IPP is a known substrate of
180 the FPPS/GGPPS, and in the primary sequence Ser228 is adjacent to conserved KT residues and
181 an Asp-rich region required for catalysis in all homologous FPPS and GGPPS enzymes (Figure
182 2C). *Pf*FPPS/GGPPS was a strong candidate for further validation as the molecular target of
183 MMV019313.
184
185 **Overexpression and an S228T variant of *Pf*FPPS/GGPPS confers resistance to**
186 **MMV019313**
187 We determined whether overexpression of wildtype *Pf*FPPS/GGPPS was sufficient to
188 confer resistance to MMV019313. A transgene encoding FPPS/GGPPS-GFP under the control of
189 either the ribosomal L2 protein (*RL2*; PF3D7_1132700) or calmodulin (*CaM*; PF3D7_1434200)
190 promoter was integrated into an engineered *att*B locus in $Dd2^{attb}$ parasites (28). Expression of the
191 CaM promoter is 10 to 50-fold greater across the life cycle than that of the RL2 promoter based
192 on RNA-seq data, resulting in appreciably greater FPPS/GGPPS-GFP protein (Figure S3A; 29).
193 Therefore, we compared the effect of no, moderate (RL2), and high (CaM) levels of
194 FPPS/GGPPS-GFP overexpression on susceptibility to MMV019313. As shown in Figure 3A,
195 overexpression of FPPS/GGPPS-GFP results in a dose-dependent increase in the EC_{50} of
196 MMV019313 with intermediate-level resistance to MMV019313 observed in the RL2-
197 FPPS/GGPPS-GFP strain and high-level resistance observed in the CaM-FPPS/GGPPS-GFP
198 strain. Notably growth inhibition by MMV019313 in the CaM-FPPS/GGPPS-GFP strain could
199 no longer be rescued by IPP, indicating that complete resistance to inhibition of the specific IPP-
200 rescuable target had been achieved (Figure S3B).

201 We also determined whether the S228T variant of GGPPS confers MMV019313
202 resistance. Initially we attempted to introduce the S228T mutation into the *fpps/ggpps* gene in the
203 *P. falciparum* genome using CRISPR-Cas9 mutagenesis but were unable to recover mutant
204 parasites. As an alternative, we overexpressed the FPPS/GGPPS(S228T)-GFP variant using the
205 "moderate" RL2 promoter and compared its effect on MMV019313 susceptibility with that of
206 the wild-type RL2-FPPS/GGPPS-GFP. Overexpression of the FPPS/GGPPS(S228T)-GFP
207 variant, even at moderate levels, caused an 18-fold increase in the EC_{50} which did not increase
208 further with IPP rescue, indicating that complete resistance to inhibition of the specific, IPP-
209 rescuable target had been achieved (Figure 3B and S3C). Because moderate overexpression of
210 the S228T variant caused greater MMV019313 resistance than moderate overexpression of
211 wildtype *Pf*FPPS/GGPPS, we conclude that the S228T variant is sufficient to confer resistance
212 independent of overexpression. Altogether these results clearly demonstrated that the
213 mechanism-of-action of MMV0193313 is dependent on *Pf*FPPS/GGPPS.
214
215 **MMV019313 specifically inhibits the enzymatic activity of *Pf*FPPS/GGPPS**
216 To confirm that *Pf*FPPS/GGPPS is the molecular target of MMV019313, we directly
217 measured MMV019313 inhibition in enzymatic assays. Consistent with a previous report,
218 purified *Pf*FPPS/GGPPS catalyzed the production of both farnesyl(C15)-PP and
219 geranylgeranyl(C20)-PP (2). To measure the inhibitory effect of MMV019313, we determined
220 its IC_{50} for FPP and GGPP production in two conditions. In the first "non-saturating" condition,
221 substrate concentrations equaled K_M values (Figure S4), the concentration at which the rate of
222 reaction is half-maximal. In the second "k_{cat}" condition, substrate concentrations were saturating
223 and the rate of reaction was maximal. Measuring inhibitor effects in both "non-saturating" and
224 "k_{cat}" conditions increases the sensitivity for detecting different types of inhibitors (competitive,
225 non-competitive, uncompetitive). We found the IC_{50} value was 330 nM for FPP production
226 under "non-saturating" conditions, comparable to its EC_{50} value in cellular growth inhibition
227 assays (Figure 1B and S5). MMV019313 was identified by its IPP rescue phenotype in cell
228 growth assays wherein addition of exogenous substrate increases enzymatic rates, indicating that
229 physiological conditions are likely sub-saturating. Therefore its IC_{50} value measured in sub-
230 saturating condition is more relevant for comparison to its EC_{50} value for growth inhibition.
231 Under "k_{cat}" conditions, IC_{50} values were 2.0 μM for FPP production and 9.8 μM for GGPP
232 production (Figure 4A-B).
233 Since inhibition was detectable in both conditions, assays of mutant and human enzymes
234 were performed at saturating conditions which gives higher signal-to-noise. Significantly
235 MMV019313 at concentrations up to 200 μM did not inhibit human FPPS or GGPPS activity,
236 indicating that it was at least 100-fold selective for *Pf*FPPS/GGPPS over human homologs
237 (Figure 4A-B). In contrast, the most selective bisphosphonate identified by a previous study,
238 BPH-703, showed only a 2.6-fold selectivity for *Pf*FPPS/GGPPS versus human FPPS and 3.6-
239 fold selectivity versus human GGPPS in enzymatic assays (Figure 4C-D; 6).
240
241 **MMV019313 binds a novel site on *Pf*FPPS/GGPPS, distinct from that of bisphosphonates**
242 The lack of inhibition of human FPPS and GGPPS by MMV019313 was intriguing since
243 *Pf*FPPS/GGPPS is structurally related to human FPPS and GGPPS and all are inhibited by
244 bisphosphonates (6). Co-crystal structures have shown that bisphosphonates, zoledronate and its
245 lipophilic analog BPH-703, bind in the allylic substrate (DMAPP, GPP, or FPP) site in the
246 *Plasmodium vivax* FPPS/GGPPS homolog (6). This binding is similar to what is observed in

247 bisphosphonate-mammalian FPPS complexes (30-33). To determine whether MMV019313 and
248 bisphosphonates share a common binding site, we compared the effect of the S228T variant on
249 inhibition by MMV019313 and the bisphosphonate BPH-703. MMV019313 and BPH-703 both
250 inhibited wild-type *Pf*FPPS/GGPPS activity. However only MMV019313 inhibition was
251 decreased by over 10-fold in the S228T variant (Figure 4A-D). This difference in their *in vitro*
252 enzyme inhibition was consistent with the effect on parasite growth inhibition, in which
253 moderate overexpression of the S228T variant conferred resistance to MMV019313 but not
254 BPH-703 (Figure S5). In addition, residue S228 is adjacent to the IPP binding site in the
255 bisphosphonate-PvFPPS/GGPPS structures and distal from the bound bisphosphonate. These
256 results demonstrate that MMV019313 has a novel binding mode, distinct from the known allylic
257 substrate site occupied by bisphosphonates, one which may confer its specificity for *Plasmodium*
258 FPPS/GGPPS over human homologs.
259 Because our biochemical results indicated that MM019313 binds a new site which is
260 unique to *Pf*FPPS/GGPPS, we performed molecular docking calculations to evaluate the
261 likelihood of MMV019313 binding at known small molecule binding sites in *Pf*FPPS/GGPPS.
262 Three small molecule binding sites have been identified in FPPS and GPPS enzymes: 1) the
263 allylic substrate binding site, which is also occupied by bisphosphonates, 2) the IPP binding site,
264 and 3) an allosteric site identified in *Hs*FPPS (34). Because both the allylic substrate and IPP
265 sites have been structurally characterized in *Pv*FPPS/GGPPS, we used the rigid body docking
266 program Glide to generate poses with MMV019313 bound to these sites and estimate the binding
267 free energy of each pose (35-37). The binding affinity estimated for the MMV019313 poses were
268 $>10^8$ weaker than bisphosphonate at the allylic site and $>10^5$ weaker than IPP at its site (Table
269 S2). Therefore, the modeling suggests that MMV019313 is unlikely to bind either the allylic
270 substrate or IPP site. We also attempted to dock MMV019313 into other potential binding
271 pockets in the *Pv*FPPS/GGPPS apo structure but with inconclusive results.
272
273 **Discussion**
274 Farnesyl and geranylgeranyl diphosphate synthase (FPPS and GGPPS) are key branch
275 point enzymes in isoprenoid biosynthesis. Human cells contain separate FPPS and GGPPS
276 enzymes. An important class of clinical drugs, nitrogen-containing bisphosphonates, inhibits
277 human FPPS in osteoclasts and block their function and proliferation (31). Because osteoclasts
278 are responsible for bone resorption, bisphosphonates are highly effective for treatment of
279 osteoporosis and other bone remodeling diseases. Bisphosphonates are chemically stable analogs
280 of inorganic pyrophosphate containing a P-C-P bond in place of the phosphodiester, which
281 accounts for both its inhibition of FPPS (acting as an analog of the allylic diphosphate substrate)
282 and its high selectivity for osteoclasts (depositing in bone mineral which is composed of calcium
283 and phosphate). Unfortunately the charge state of bisphosphonates is a major liability in other
284 therapeutic applications, as they are poorly bioavailable, rapidly cleared by the kidney, and do
285 not achieve therapeutic levels in serum for treatment of non-bone diseases (5, 8, 25, 38).
286 *Pf*FPPS/GGPPS, the molecular target of MMV019313 as demonstrated in this study,
287 closely resembles mammalian FPPS enzymes in sequence, structure, and inhibition by
288 bisphosphonates (2, 6). Like human FPPS, it is a central node in cellular isoprenoid biosynthesis
289 vulnerable to drug inhibition (4, 31, 39). In *Plasmodium*, FPP and GGPP are required for the
290 biosynthesis of prenylated proteins, the prenyl modification of ubiquinone, and other isoprenoid
291 products, such that inhibition of *Pf*FPPS/GGPPS disrupts multiple cellular pathways (3, 40-43).
292 Previously lipophilic bisphosphonates modified with an alkyl chain to increase their cell

293 permeability were shown to inhibit *Pv*FPPS/GGPPS homolog and clear both blood- and liver-
294 stage *Plasmodium* parasites in mice infection models (5, 6). Importantly, these results validated
295 *Plasmodium* FPPS/GGPPS as an antiparasitic drug target for both acute malaria treatment and
296 malaria chemoprophylaxis.
297 Our identification of MMV019313 further addresses two key hurdles in the development
298 of *Pf*FPPS/GGPPS inhibitors as antimalarial drugs. First, MMV019313 represents the first non-
299 bisphosphonate class of *Plasmodium* FPPS/GGPPS inhibitors with superior physicochemical
300 properties. Many efforts have been made to develop modified bisphosphonates or non-
301 bisphosphonate compounds as FPPS and/or GGPPS inhibitors for treatment of soft-tissue
302 cancers and infectious diseases (34, 44-47). Unlike bisphosphonates, MMV019313 has drug-like
303 physicochemical properties satisfying the Rule of 5 and does not need to mimic a charged
304 diphosphate substrate to achieve FPPS/GGPPS inhibition (25). As a compound in the Malaria
305 Box library, it has already been tested in a panel of bioactivity and pharmacokinetic assays with
306 encouraging results (25). Furthermore the results of >300 assays characterizing Malaria Box
307 compounds as part of an innovative "open source" drug discovery effort by many groups will be
308 a rich source of information (25, 48-50).
309 Second, MMV019313 has high selectivity for *Pf*FPPS/GGPPS over human FPPS and
310 GGPPS, minimizing the potential for mechanism-based (e.g. "on-target") toxicity. In fact, we
311 could not detect any inhibition of human FPPS or GGPPS indicating selectivity at the enzymatic
312 level of at least 100-fold. Consistent with this lack of enzymatic inhibition, MMV019313
313 showed no cytotoxity against a panel of 60 human cancer cell lines at 10 μM (25). In contrast,
314 the most selective bisphosphonate BPH-703 identified by No *et al* showed 2.6-3.6-fold
315 selectivity in our enzymatic assays (corresponding to a reported therapeutic index of 193 in
316 growth inhibition assays; 6). Our results suggest that MMV019313 binds a novel site in
317 *Pf*FPPS/GGPPS that is either absent from or substantially different in the human homologs,
318 which may explain its high selectivity. Altogether MMV019313 offers a distinct and promising
319 starting point for development of antimalarial FPPS/GGPPS inhibitors, which circumvents the
320 inherent liabilities of the bisphosphonate pharmacophore and greatly improves on their
321 selectivity.
322 Our immediate priority is to obtain structures of the inhibitor-enzyme complex to aid in
323 structure-based design of MMV019313 derivatives with higher potency, as well as discovery of
324 additional chemical scaffolds that occupy this new binding site. A potential challenge is that the
325 FPPS structure is dynamic during catalysis. For example, the human FPPS is known to undergo
326 at least two critical conformational changes (31): The first is from an "open" apo form to a
327 "closed" conformation upon binding of the allylic substrate, which is associated with drastically
328 increased affinity for the allylic substrate (and bisphosphonates that mimic this substrate) as well
329 as orders the IPP binding pocket. The second structural change occurs upon IPP binding and
330 sequesters the active site from bulk solvent. Several attempts to obtain co-crystal structures of
331 MMV019313 with *Pv*FPPS/GGPPS under conditions in which bisphosphonate-*Pv*FPPS/GGPPS
332 crystals were obtained (presumed to correspond to the "closed" conformation) have been
333 unsuccessful (personal communication, Dr. Raymond Hui). Additional crystallization conditions
334 may require testing in the presence and absence of different allylic substrates and IPP, as their
335 binding could affect the binding of MMV019313. Given the dynamic and complex mechanism
336 of FPPS and GGPPS enzymes, detailed kinetic characterization of MMV019313 inhibition will
337 be important to complement structural studies.

338 Since the S228T variant distinguishes between MMV019313 and bisphosphonate binding
339 to *Pf*FPPS/GGPPS, obtaining its structure to compare with wildtype FPPS/GGPPS will also offer
340 clues to this new mode-of-inhibition. The resistance caused by the S228T variant could be
341 explained by a direct contact between Ser228 and MMV019313 in a new small molecule binding
342 pocket. But because the change from Ser to Thr is quite conservative, the addition of a methyl
343 group, it seems more likely that Ser228 is involved in conformational dynamics important for
344 catalysis. Structural analysis of this variant enzyme may reveal altered conformational states
345 underlying the resistance to MMV019313.
346 Optimization of the bioactivity and pharmacokinetic properties of MMV019313
347 derivatives will be priorities for their development as antimalarials. The luciferase-based
348 enzymatic assays performed in our study are robust for detection of effective inhibitors and can
349 be adapted to high-throughput screening of small molecule libraries (in contrast we found a
350 commercially-available colorimetric assay was not sufficiently sensitive; 51). Inhibitor-enzyme
351 structures will greatly accelerate optimization for potency against the *Plasmodium*
352 FPPS/GGPPS, while simultaneously minimizing binding to the human homologs. *P. falciparum*
353 strains overexpressing wildtype or the S228T variant, generated during this study, can also be re-
354 tooled as secondary cellular assays for on-target specificity. The drug properties of MMV019313
355 derivatives will be optimized in standard absorption-distribution-metabolism-excretion-toxicity
356 (ADME-T) assays. For example, we found that while MMV019313 is stable to human liver
357 microsomal enzymes ($t_{½}$> 159 min), its $t_{½}$ in mouse liver microsomes was 4 min. This metabolic
358 instability may account for a <1μM peak serum concentration following oral administration in
359 mice and will need to be addressed before derivatives can be tested in mouse models of
360 *Plasmodium* infection (25).
361 Finally, our study demonstrates two methodological improvements. First, we took
362 advantage of a quantitative screen for IPP chemical rescue using a range of inhibitor
363 concentrations, rather than a single high dose. The increased sensitivity allowed us to identify
364 MMV019313, though it was missed in prior screens. It also permits the screen to be performed
365 with geranylgeraniol, which is significantly less costly than IPP, since so far all identified
366 inhibitors that rescue with IPP also show at least a partial rescue of parasite growth inhibition
367 with geranylgeraniol (24, 52). Second, we employed chemical mutagenesis to select for drug-
368 resistant mutants, which has not previously been reported in *Plasmodium* to our knowledge but
369 has been used for genetic screens in *Toxoplasma gondii* (27). Notably we were unable to select
370 MMV019313-resistant parasites in the absence of chemical mutagenesis, though this same
371 protocol was effective in selecting drug resistance against MMV008138 when performed in
372 parallel (23). Our experience suggests that the use of chemical mutagens will increase successful
373 selection for drug resistance in *Plasmodium* parasites, which is the most common method
374 employed to identify drug targets from phenotypic drug screens (18-20). The low frequency of *in*
375 *vitro* MMV019313 resistance also indicates that clinical resistance will also be less frequent to
376 MMV019313 and its derivatives.
377
378
379 **Methods**
380
381 ***P. falciparum in vitro* cultures.** *Plasmodium falciparum* W2 (MRA-157) and Dd2^{attB}
382 (MRA-843) were obtained from MR4. Parasites were grown in human erythrocytes (2%
383 hematocrit) in RPMI 1640 media supplemented with 0.25% Albumax II (GIBCO Life

384 Technologies), 2 g/L sodium bicarbonate, 0.1 mM hypoxanthine, 25 mM HEPES (pH 7.4), and
385 50 µg/L gentamycin, at 37°C, 5% O_2, and 5% CO_2. For passage of drug-treated, IPP-rescued
386 parasites, the media was supplemented with 5 µM drug and 200 µM IPP (Isoprenoids LC or
387 NuChem). For comparison of growth between different treatment conditions, cultures were
388 carried simultaneously and handled identically with respect to media changes and addition of
389 blood cells
390
391 **Chemical handling.** Malaria Box compounds were received as 10 mM DMSO stocks in
392 96-well plates and diluted three-fold manually in DMSO. Fosmidomycin was included in control
393 wells. Two-fold serial dilutions of the 96-well plates were performed on Velocity11. Compound
394 stocks stored in DMSO were diluted for growth assays. MMV019313 was purchased from
395 ChemDiv
396
397 **qHTS screen for IPP chemical rescue.** Growth assays were performed in 384-well clear
398 bottom assay plates (E and K scientific, Santa Clara, CA). Drug (100-400 nL) was added directly
399 to each well using PinTool (V&P Scientific) on a Sciclone ALH3000 (Caliper Sciences). Using
400 the Titertek Multidrop 384, first 40 µL of growth media with and without 375 µM IPP was
401 dispensed, followed by 10 µL ring-stage *P. falciparum* D10 parasites (parasitemia 0.8% in 10%
402 hematocrit) into 384-well plates using the Titertek Multidrop 384. The final assay consisted of
403 50 µL ring-stage cultures at 0.8% parasitemia/ 2% hematocrit and drug concentrations from
404 0.01-26.7 µM ± 300 µM IPP. The plate was incubated at 37°C for 72 h. Parasites were lysed
405 with 10 µL 5mM EDTA, 1.6% Triton-X, 20mM Tris-HCl and 0.16% Saponin containing 0.1%
406 Sybr Green I (Invitrogen). The plates were then incubated at -80 ^{o}C for 20 min and thawed at
407 room temperature overnight in the dark. Fluorescence was detected using Flexstation II- 384.
408 Compounds that showed IPP rescue of growth inhibition at 1 or more drug concentrations in the
409 initial 384-well high-throughput screen were re-tested in a 96-well growth assay.
410
411 **Growth inhibition assays to determine EC_{50} values.** *P. falciparum* cultures (125 µL)
412 were grown in 96-well plates containing serial dilution of drugs in triplicate. Media was
413 supplemented with 200 µM IPP as indicated. Growth was initiated with ring-stage parasites at
414 1% parasitemia and 0.5% hematocrit. Plates were incubated for 72h. Growth was terminated by
415 fixation with 1% formaldehyde and parasitized cells were stained with 50 nM YOYO-1
416 (Invitrogen). Parasitemia was determined by flow cytometry. Data were analyzed by BD C6
417 Accuri C-Sampler software, and EC_{50} curves plotted by GraphPad Prism.
418
419 ***P. falciparum* mutagenesis and resistance selection.** Late-stage parasites were purified
420 using a SuperMACS II separator (Miltenyi Biotec) and incubated in complete medium with 8.3 –
421 2025 µM ethyl methanesulfonate (EMS, 6 concentrations total) for 2 hours. The concentrations
422 of EMS used were selected by determining the EC_{50} in 72h parasite growth inhibition assays.
423 The highest concentration used for mutagenesis was equal to the EC_{50} in order to maximize the
424 selection pressure. The mutagen was then serially diluted 1:3 to test lower concentrations that
425 might give lower mutation rates and therefore a lower frequency of passenger mutations.
426 Mutagenized parasites were washed and separated into wells of 10 mL total volume
427 (approximately 10% parasitemia, 2 % HCT). MMV019313 drug selection was applied to one
428 well for each mutagenesis condition at 600 nM (approximately EC_{75}), while the other well was
429 left untreated in order to serve as a control for whole genome sequencing. Parasites were fed

430 daily for the first week and every 3 days thereafter. Each culture was split in half every 6 days in
431 order to introduce fresh RBC. Drug pressure was maintained for 32 days, with no observable
432 parasite growth. After 32 days of selection, half of the culture from each EMS condition was
433 removed from drug pressure. In these cultures, parasites which showed resistance to
434 MMV019313 by a standard drug assay were observable after 7 days at all EMS conditions used.
435 The parasites treated with the two lowest concentrations of EMS were selected for whole
436 genome sequencing.
437
438 **Whole Genome Sequencing.** *Plasmodium falciparum* strains were sequenced by
439 Illumina sequencing as described previously (53). Briefly, NEBNext DNA library reagents
440 (NEB) and NEXTflex DNA barcode adapters (Bioo Scientific) were used to prepare PCR-free
441 libraries (54). Eight whole genome gDNA libraries were multiplexed and spiked with 8% PhiX
442 control. Single-end sequencing was performed across two lanes on an Illumina HiSeq 2500
443 system. Data was analyzed using tools available in the Galaxy platform (55-57). Sequencing
444 reads were mapped against the *P. falciparum* 3D7v.10.0 reference genome using the Burrows-
445 Wheeler Alignment tool (58). Sequencing data was visualized using Integrative Genomics
446 Viewer (IGV) (59, 60). Variants were called using Freebayes (61) and filtered for Quality >100
447 and Read Depth >30 using GATK tools (62). SnpEff was used to annotate the list of variants
448 based on the *P. falciparum* 3D7v9.1 reference genome (63). Sequencing data have been
449 deposited to the SRA.
450
451 ***P. falciparum* Transfections.** An *E. coli* codon optimized version of *Pf*FPPS/GGPPS
452 (PF3D7_1128400) was designed and synthesized by GeneWiz. Quick change mutagenesis was
453 used to mutate GGPPS serine 228 to a threonine in the pUC vector provided by GeneWiz. These
454 constructs were then moved into the pLN transfection plasmid designed for Bxb1
455 mycobacteriophage integrase system (64). The In-fusion cloning kit (Clontech) was used for all
456 cloning. Restriction enzymes *Av*rII and *Bs*iWI were used to linearize the pLN vector. GGPPS
457 was designed to have a *C*-terminal GFP tag. All transgenes were driven with either the ribosomal
458 L2 protein (RL2) promoter (PF3D7_1132700) or the calmodulin (CaM) promoter
459 (PF3D7_1434200) as denoted.
460 Transfections were carried out as previously described (65). Briefly, 400 µL fresh red
461 blood cells were preloaded with 100 µg of both pINT, which carries the bacteriophage integrase,
462 and pRL2, which carries the gene of interest and the blasticidin resistance cassette, using a
463 BioRad Gene-Pulser Xcell Electroporator. Electroporation conditions were infinite resistance,
464 310 V, and 950 µF using a 2 mm cuvette. Preloaded red blood cells were combined with 2.5 mL
465 ~20% schizont $Dd2^{attB}$ parasites and allowed to recover for 2 days before selection pressure was
466 applied. Transfected parasites were selected with 2.5 µg/mL blasticidin are were detectable by
467 thin smear within 15 days. Integration was confirmed by PCR and identity of the transgene was
468 confirmed by sanger sequencing.
469
470 **Immunoblots.** Parasites expressing either ACP_L-GFP or one of the FPPS/GGPPS
471 constructs generated in this study were isolated by saponin lysis and resuspended in 1xNuPage
472 LDS sample buffer (Invitrogen). Whole cell lysate was separated by SDS-PAGE using 4-12%
473 Bis-Tris gels (Initrogen) and transferred to nitrocellulose using a Trans Turbo-blot (BioRad).
474 Membranes were blocked with 3% BSA, probed with 1:5,000 monoclonal anti-GFP JL-8

475 (BioRad) overnight, washed, then probed with 1:10,000 IRDye 680LT goat-anti-mouse. The
476 Western was imaged using a Oddysey Imager (LiCor Biosciences).
477
478 **Live microscopy.** Infected red blood cells were treated with Hoescht to stain the nucleus.
479 Single z-stack images were collected on an epifluorescence Nikon eclipse.
480
481 **Quantative PCR.** Quantitative PCR was performed as previously published(21). Briefly,
482 parasites from 200 µL of culture were isolated by saponin lysis followed by PBS wash to remove
483 extracellular DNA. DNA was purified using DNeasy Blood and Tissue kit (Qiagen). Primers
484 were designed to target genes found on the apicoplast or nuclear genome: *tufA* (apicoplast) 5′-
485 GATATTGATTCAGCTCCAGAAGAAA-3′ / 5′-ATATCCATTTGTGTGGCTCCTATAA-3′
486 and *CHT1* (nuclear) 5′-TGTTTCCTTCAACCCCTTTT-3′ / 5′-TGTTTCCTTCAACCCCTTTT-
487 3′. Reactions contained template DNA, 0.15 µM of each primer, and 0.75× LightCycler 480
488 SYBR Green I Master mix (Roche). PCR reactions were performed at 56°C primer annealing
489 and 65°C template extension for 35 cycles on a Lightcycler 6500 (Roche). For each time point,
490 the apicoplast：nuclear genome ratio of the fosmidomycin-treated positive control,
491 chloramphenicol-treated negative control, or MMV019313-treated experiment were calculated
492 relative to that of an untreated control collected at the same time.
493
494 **Recombinant protein purification.** Full length constructs of *Pf*FPPS/GGPPS, *Hs*FPPS,
495 and *Hs*GGPPS were cloned into pET28a with an n-terminal hexahistidine tag. The *P. falciparum*
496 FPPS/GGPPS was codon optimized for expression in *E. coli* (GeneWiz). *Pf*FPPS/GGPPS was
497 mutagenized (S228T) using quick change mutagenesis. When expressed in *E. coli,*
498 *Pf*FPPS/GGPPS (wt and S228T) and *Hs*FPPS were toxic. Cultures were supplemented with 0.4%
499 glucose and grown to OD_{600} of 0.8-1 and induced with 0.5 mM IPTG. *Hs*GGPPS was grown
500 without supplementation to an OD_{600} of 0.8-1. All cultures were induced for 4 hours at 37 °C,
501 then harvested. Cells were lysed in 20 mM HEPES pH 8.0, 150 mM NaCl, 2 mM $MgCl_2$, and
502 protease inhibitor cocktail using sonication. Cleared lysates were either mixed with Talon metal
503 affinity resin (Clonetech) or purified over 5 ml HisTrap columns (GE Healthcare). His tagged
504 protein was purified with a single step purification eluting with buffer with 300 mM imidazole.
505 Proteins were dialyzed to remove imidazole and flash frozen.
506
507 ***In vitro* FPPS/GGPPS assays.** FPPS/GGPPS activity was measured by monitoring
508 pyrophosphate release using the Lonza PPiLight kit under kinetic conditions. Drug and either 20
509 µg/ml *Pf*FPPS/GGPPS, 40 µg/ml *Hs*GGPPS, or 100 µg/ml *Hs*FPPS protein were incubated for
510 30 min room temperature. The reaction was initiated by the addition of Lonza PPiLight kit
511 reaction mix and substrates. Saturating substrate conditions were 100 µM GPP or FPP, and 200
512 µM IPP. Sub-saturation conditions were K_M conditions as shown in Figure S4. Luciferase
513 activity was monitored overtime using a BioTeck plate reader.
514
515 **MMV019313 ligand docking.** Using a solved *Pv*FPPS/GGPPS structure (PDB: 3EZ3,
516 zoledronate and IPP bound) as a receptor model protein preparation wizard was used to add back
517 in missing hydrogens and side chains. All crystallographic waters were removed. Hydrogen
518 bonds were calculated using Epik at pH 8 (±1). The protein structure was minimized using OPL3
519 force field. MMV019313 was docked using glide to receptor grids generated from the relevant
520 crystallized small molecules.

Acknowledgements

We are grateful to Medicines for Malaria Ventures (MMV) for providing the Malaria Box compounds and making this valuable library freely available, as well as GlaxoSmithKline for their screening efforts that first identified MMV019313 (TCMDC-123889). We would like to thank Dr. Susmitha Suresh for performing drug screens and Dr. Felice Kelly for advice on how to chemically mutagenize our parasites for resistance selection. We are grateful to Dr. James Dunford (University of Oxford) for advice in developing the *in vitro* enzyme activity assays. We also would like to acknowledge Dr. Wei Zhu and Professor Eric Oldfield (University of Illinois, Urbana-Champaign) for *in vitro P. vivax* GGPPS activity assays and providing BPH-703.

Financial Disclosure

Funding support for this project was provided by the Stanford Consortium for Innovation, Design, Evaluation and Action (C-IDEA), NIH 1K08AI097239 (EY), NIH 1DP5OD012119 (EY), the Burroughs Wellcome Fund Career Award for Medical Scientists (EY), the Burroughs Wellcome Fund Investigators in Pathogenesis of Infectious Disease (PATH) Award (ML), and the Stanford School of Medicine Dean's Postdoctoral Fellowship (JEG).

References

1. Jomaa H, et al. (1999) Inhibitors of the nonmevalonate pathway of isoprenoid biosynthesis as antimalarial drugs. *Science* 285(5433):1573–1576.

2. Jordão FM, et al. (2013) Cloning and characterization of bifunctional enzyme farnesyl diphosphate/geranylgeranyl diphosphate synthase from *Plasmodium falciparum*. *Malar J* 12(1):184.

3. Tonhosolo R, et al. (2005) Identification, molecular cloning and functional characterization of an octaprenyl pyrophosphate synthase in intra-erythrocytic stages of *Plasmodium falciparum*. *Biochem J* 392(Pt 1):117–126.

4. Artz JD, et al. (2011) Molecular characterization of a novel geranylgeranyl pyrophosphate synthase from *Plasmodium* parasites. *J Biol Chem* 286(5):3315–3322.

5. Singh AP, et al. (2010) Lipophilic bisphosphonates are potent inhibitors of *Plasmodium* liver-stage growth. *Antimicrob Agents Chemother* 54(7):2987–2993.

6. No JH, et al. (2012) Lipophilic analogs of zoledronate and risedronate inhibit *Plasmodium* geranylgeranyl diphosphate synthase (GGPPS) and exhibit potent antimalarial activity. *Proc Natl Acad Sci USA* 109(11):4058–4063.

7. Michael B Martin, et al. (2001) Bisphosphonates Inhibit the Growth of *Trypanosoma brucei, Trypanosoma cruzi, Leishmania donovani, Toxoplasma gondii,* and *Plasmodium falciparum*: A Potential Route to Chemotherapy. *J Med Chem* 44(6):909–916.

561 8. Jordão FM, et al. (2011) In vitro and in vivo antiplasmodial activities of risedronate and
562 its interference with protein prenylation in *Plasmodium falciparum*. *Antimicrob Agents*
563 *Chemother* 55(5):2026–2031.

564 9. Ghosh S, et al. (2004) Effects of bisphosphonates on the growth of *Entamoeba histolytica*
565 and *Plasmodium* species in vitro and in vivo. *J Med Chem* 47(1):175–187.

566 10. Nallan L, et al. (2005) Protein farnesyltransferase inhibitors exhibit potent antimalarial
567 activity. *J Med Chem* 48(11):3704–3713.

568 11. Eastman RT, et al. (2007) Resistance mutations at the lipid substrate binding site of
569 *Plasmodium falciparum* protein farnesyltransferase. *Mol Biochem Parasitol* 152(1):66–71.

570 12. Eastman RT, et al. (2005) Resistance to a protein farnesyltransferase inhibitor in
571 *Plasmodium falciparum*. *J Biol Chem* 280(14):13554–13559.

572 13. Fernandes JF, et al. (2015) Fosmidomycin as an antimalarial drug: a meta-analysis of
573 clinical trials. *Future Microbiol* 10(8):1375–1390.

574 14. Sinigaglia L, Varenna M, Casari S (2007) Pharmacokinetic profile of bisphosphonates in
575 the treatment of metabolic bone disorders. *Clin Cases Miner Bone Metab* 4(1):30–36.

576 15. Van Voorhis WC, et al. (2007) Efficacy, pharmacokinetics, and metabolism of
577 tetrahydroquinoline inhibitors of *Plasmodium falciparum* protein farnesyltransferase.
578 *Antimicrob Agents Chemother* 51(10):3659–3671.

579 16. Tsuchiya T, et al. (1982) Pharmacokinetics and metabolism of fosmidomycin, a new
580 phosphonic acid, in rats and dogs. *Eur J Drug Metab Pharmacokinet* 7(1):59–64.

581 17. Spangenberg T, et al. (2013) The open access malaria box: a drug discovery catalyst for
582 neglected diseases. *PLoS ONE* 8(6):e62906.

583 18. Rottmann M, et al. (2010) Spiroindolones, a potent compound class for the treatment of
584 malaria. *Science* 329(5996):1175–1180.

585 19. Gamo FJ, et al. (2010) Thousands of chemical starting points for antimalarial lead
586 identification. *Nature* 465(7296):305–310.

587 20. Guiguemde WA, et al. (2010) Chemical genetics of *Plasmodium falciparum*. *Nature*
588 465(7296):311–315.

589 21. Yeh E, Derisi JL (2011) Chemical rescue of malaria parasites lacking an apicoplast
590 defines organelle function in blood-stage *Plasmodium falciparum*. *PLoS Biol*
591 9(8):e1001138.

592 22. Bowman JD, et al. (2014) Antiapicoplast and gametocytocidal screening to identify the
593 mechanisms of action of compounds within the malaria box. *Antimicrob Agents*
594 *Chemother* 58(2):811–819.

595 23. Wu W, et al. (2015) A chemical rescue screen identifies a *Plasmodium falciparum*
596 apicoplast inhibitor targeting MEP isoprenoid precursor biosynthesis. *Antimicrob Agents*
597 *Chemother* 59(1):356–364.

598 24. DeRisi JL, et al. (2014) *UCSF DeRisi Lab MMV Box Apicoplast Screening* (EMBL-EBI)
599 doi:10.6019/CHEMBL2448809.

600 25. Van Voorhis WC, et al. (2016) Open Source Drug Discovery with the Malaria Box
601 Compound Collection for Neglected Diseases and Beyond. *PLoS Pathog* 12(7):e1005763.

602 26. Amberg-Johnson K, Ganesan SM, Lorenzi HA, Niles JC, Yeh E (2017) A first-in-class
603 inhibitor of parasite FtsH disrupts plastid biogenesis in human pathogens. *bioRxiv*:108910.

604 27. Franco M, et al. (2016) A Novel Secreted Protein, MYR1, Is Central to Toxoplasma's
605 Manipulation of Host Cells. *MBio* 7(1):e02231–15.

606 28. Nkrumah LJ, et al. (2006) Efficient site-specific integration in *Plasmodium falciparum*
607 chromosomes mediated by mycobacteriophage Bxb1 integrase. *Nat Methods* 3(8):615–
608 621.

609 29. Otto TD, et al. (2010) New insights into the blood-stage transcriptome of *Plasmodium*
610 *falciparum* using RNA-Seq. *Mol Microbiol* 76(1):12–24.

611 30. Rondeau J-M, et al. (2006) Structural Basis for the Exceptional in vivo Efficacy of
612 Bisphosphonate Drugs. *ChemMedChem* 1(2):267–273.

613 31. Kavanagh KL, et al. (2006) The molecular mechanism of nitrogen-containing
614 bisphosphonates as antiosteoporosis drugs. *Proc Natl Acad Sci USA* 103(20):7829–7834.

615 32. Zhang Y, et al. (2013) Chemo-Immunotherapeutic Anti-Malarials Targeting Isoprenoid
616 Biosynthesis. *ACS Med Chem Lett* 4(4):423–427.

617 33. Yokoyama T, et al. (2015) Protonation State and Hydration of Bisphosphonate Bound to
618 Farnesyl Pyrophosphate Synthase. *J Med Chem* 58(18):7549–7556.

619 34. Jahnke W, et al. (2010) Allosteric non-bisphosphonate FPPS inhibitors identified by
620 fragment-based discovery. *Nat Chem Biol* 6(9):660–666.

621 35. Halgren TA, et al. (2004) Glide: a new approach for rapid, accurate docking and scoring.
622 2. Enrichment factors in database screening. *J Med Chem* 47(7):1750–1759.

623 36. Friesner RA, et al. (2004) Glide: a new approach for rapid, accurate docking and scoring.
624 1. Method and assessment of docking accuracy. *J Med Chem* 47(7):1739–1749.

625 37. Friesner RA, et al. (2006) Extra precision glide: docking and scoring incorporating a
626 model of hydrophobic enclosure for protein-ligand complexes. *J Med Chem* 49(21):6177–
627 6196.

628 38. Cremers SCLM, Pillai G, Papapoulos SE (2005) Pharmacokinetics/pharmacodynamics of
629 bisphosphonates: use for optimisation of intermittent therapy for osteoporosis. *Clin*
630 *Pharmacokinet* 44(6):551–570.

631 39. Luckman SP, et al. (1998) Nitrogen-containing bisphosphonates inhibit the mevalonate
632 pathway and prevent post-translational prenylation of GTP-binding proteins, including
633 Ras. *J Bone Miner Res* 13(4):581–589.

634 40. de Macedo CS, Uhrig ML, Kimura EA, Katzin AM (2002) Characterization of the
635 isoprenoid chain of coenzyme Q in *Plasmodium falciparum*. *FEMS Microbiol Lett*
636 207(1):13–20.

637 41. Tonhosolo R, et al. (2009) Carotenoid biosynthesis in intraerythrocytic stages of
638 *Plasmodium falciparum*. *J Biol Chem* 284(15):9974–9985.

639 42. Gabriel HB, et al. (2015) Squalestatin is an inhibitor of carotenoid biosynthesis in
640 *Plasmodium falciparum*. *Antimicrob Agents Chemother* 59(6):3180–3188.

641 43. Chakrabarti D, et al. (2002) Protein farnesyltransferase and protein prenylation in
642 *Plasmodium falciparum*. *J Biol Chem*. doi:10.1074/jbc.M202860200.

643 44. Chen S-H, Lin S-W, Lin S-R, Liang P-H, Yang J-M (2013) Moiety-linkage map reveals
644 selective nonbisphosphonate inhibitors of human geranylgeranyl diphosphate synthase. *J*
645 *Chem Inf Model* 53(9):2299–2311.

646 45. Liu J, et al. (2014) Syntheses and characterization of non-bisphosphonate quinoline
647 derivatives as new FPPS inhibitors. *Biochim Biophys Acta* 1840(3):1051–1062.

648 46. Marzinzik AL, et al. (2015) Discovery of Novel Allosteric Non-Bisphosphonate Inhibitors
649 of Farnesyl Pyrophosphate Synthase by Integrated Lead Finding. *ChemMedChem*
650 10(11):1884–1891.

651 47. Zhang Y, et al. (2009) Lipophilic bisphosphonates as dual farnesyl/geranylgeranyl
652 diphosphate synthase inhibitors: an X-ray and NMR investigation. *J Am Chem Soc*
653 131(14):5153–5162.

654 48. Ullah I, Sharma R, Biagini GA, Horrocks P (2017) A validated bioluminescence-based
655 assay for the rapid determination of the initial rate of kill for discovery antimalarials. *J*
656 *Antimicrob Chemother* 72(3):717–726.

657 49. Allman EL, Painter HJ, Samra J, Carrasquilla M, Llinás M (2016) Metabolomic Profiling
658 of the Malaria Box Reveals Antimalarial Target Pathways. *Antimicrob Agents Chemother*
659 60(11):6635–6649.

660 50. Paul AS, Moreira CK, Elsworth B, Allred DR, Duraisingh MT (2016) Extensive Shared
661 Chemosensitivity between Malaria and Babesiosis Blood-Stage Parasites. *Antimicrob*
662 *Agents Chemother* 60(8):5059–5063.

663 51. Crowther GJ, et al. (2011) Identification of inhibitors for putative malaria drug targets
664 among novel antimalarial compounds. *Mol Biochem Parasitol* 175(1):21–29.

665 52. Zhang B, et al. (2011) A second target of the antimalarial and antibacterial agent
666 fosmidomycin revealed by cellular metabolic profiling. *Biochemistry* 50(17):3570–3577.

667 53. Straimer J, et al. (2012) Site-specific genome editing in *Plasmodium falciparum* using
668 engineered zinc-finger nucleases. *Nat Methods* 9(10):993–998.

669 54. Kozarewa I, et al. (2009) Amplification-free Illumina sequencing-library preparation
670 facilitates improved mapping and assembly of (G+C)-biased genomes. *Nat Methods*
671 6(4):291–295.

672 55. Giardine B, et al. (2005) Galaxy: a platform for interactive large-scale genome analysis.
673 *Genome Res* 15(10):1451–1455.

674 56. Blankenberg D, et al. (2010) Galaxy: a web-based genome analysis tool for
675 experimentalists. *Curr Protoc Mol Biol* Chapter 19:Unit 19.10.1–21.

676 57. Goecks J, Nekrutenko A, Taylor J, Galaxy Team (2010) Galaxy: a comprehensive
677 approach for supporting accessible, reproducible, and transparent computational research
678 in the life sciences. *Genome Biol* 11(8):R86.

679 58. Li H, Durbin R (2009) Fast and accurate short read alignment with Burrows-Wheeler
680 transform. *Bioinformatics* 25(14):1754–1760.

681 59. Robinson JT, et al. (2011) Integrative genomics viewer. *Nat Biotechnol* 29(1):24–26.

682 60. Thorvaldsdóttir H, Robinson JT, Mesirov JP (2013) Integrative Genomics Viewer (IGV):
683 high-performance genomics data visualization and exploration. *Brief Bioinformatics*
684 14(2):178–192.

685 61. Garrison E, Marth G Haplotype-based variant detection from short-read sequencing.
686 *httpsarxivorgabsv* 2012.

687 62. Van der Auwera GA, et al. (2013) From FastQ data to high confidence variant calls: the
688 Genome Analysis Toolkit best practices pipeline. *Curr Protoc Bioinformatics* 43:11.10.1–
689 33.

690 63. Cingolani P, et al. (2012) Using *Drosophila melanogaster* as a Model for Genotoxic
691 Chemical Mutational Studies with a New Program, SnpSift. *Front Genet* 3:35.

692 64. Adjalley SH, Lee MCS, Fidock DA (2010) A method for rapid genetic integration into
693 *Plasmodium falciparum* utilizing mycobacteriophage Bxb1 integrase. *Methods Mol Biol*
694 634:87–100.

695 65. Spalding MD, Allary M, Gallagher JR, Prigge ST (2010) Validation of a modified method
696 for Bxb1 mycobacteriophage integrase-mediated recombination in *Plasmodium*

falciparum by localization of the H-protein of the glycine cleavage complex to the mitochondrion. *Mol Biochem Parasitol* 172(2):156–160.

Tables

Table 1. Summary of mutations identified by whole genome sequencing

Gene ID[a]	Description[b]	Base Call[c]			AA change	Population	Read Number[d]		%[e]	
		Position	WT	EMS			WT1	R	WT2	R
PF3D7_1128400	Geranylgeranyl pyrophosphate synthase (GGPPS)	682	T	A	S228T	019313R1	219	163	100	100
						019313R2	186	181	100	62.4

[a] PlasmoDB gene Identification number
[b] Basic gene description based on PlasmoDB functional assignments
[c] WT calls match 3D7 reference genome
[d] Read depth corresponding to WT call (IGV) and Mut call (SnpEff) respectively
[e] Percent of reads corresponding to WT call (IGV) and Mut call (SnpEff) respectively

Figures and figure legends

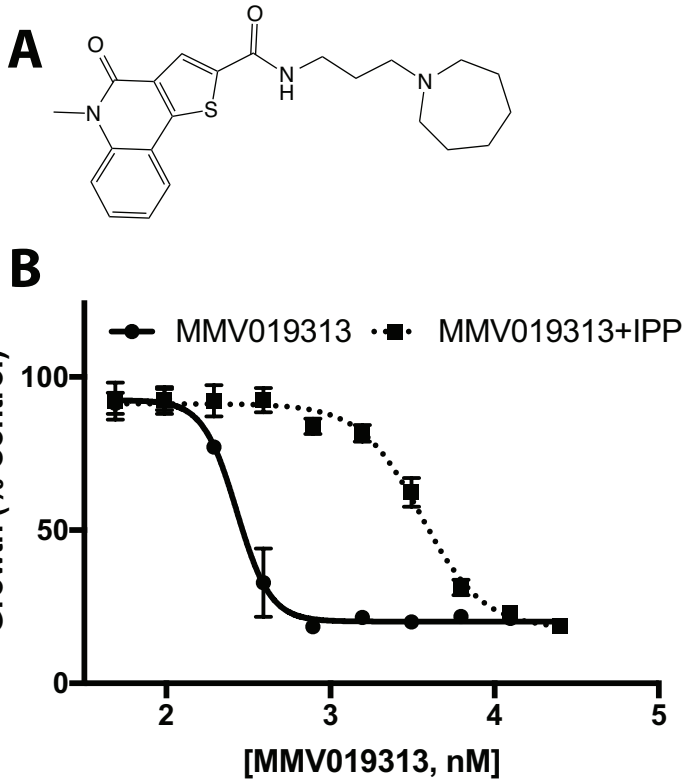

713 **Figure 1. IPP rescues growth inhibition by MMV019313. A.** The structure of MMV019313.
714 **B.** EC_{50} curves in the absence (solid line) and presence (dotted line) of IPP. Parasitemia is
715 normalized to that of an untreated control.
716
717
718

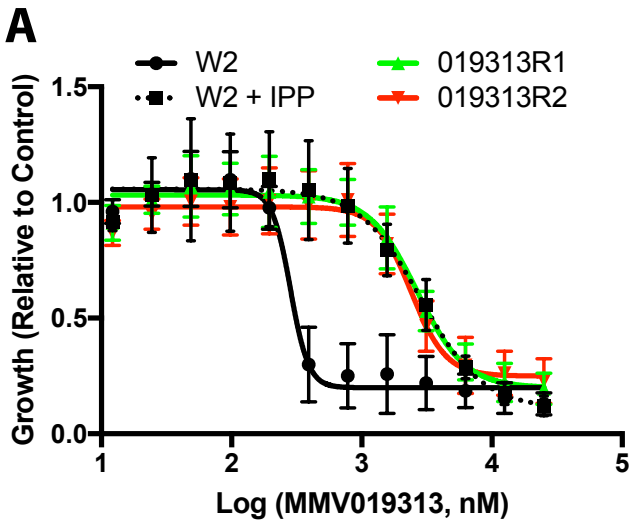

Strain	Fold Change EC_{50}
W2 + 200 µM IPP	10.06
019313R1	9.42
019313R2	8.45

B

WT	TAT	TAT	**T**CA	TTC	TTT
Control	Y	Y	**S**	F	F
019313R1/	TAT	TAT	**A**CA	TTC	TTT
R2	Y	Y	**T**	F	F

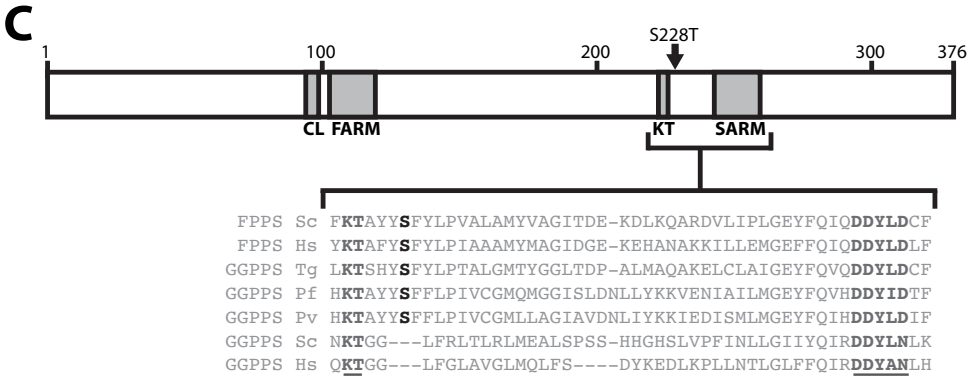

719
720 **Figure 2. MMV019313-resistant parasites contain a mutation in the bifunctional farnesyl**
721 **and geranylgeranyl diphosphate synthase. A.** EC_{50} curves of parental W2 parasites alone
722 (black, solid line) and with IPP supplementation (black, dotted line) and the two resistant
723 populations (019313R1, red line, and 019313R2, green line) without IPP added. Fold change in
724 EC_{50} compared to W2 parasites is shown in the right. **B**. Mutation determined by whole genome
725 sequencing of resistant populations 019313R1 and 019313R2, highlighted in red **C.** Schematic
726 of *Pf*FPPS/GGPPS protein. The S228T residue is highlighted in bold black while conserved KT
727 and SARM residues are highlighted in bold grey and underlined.
728

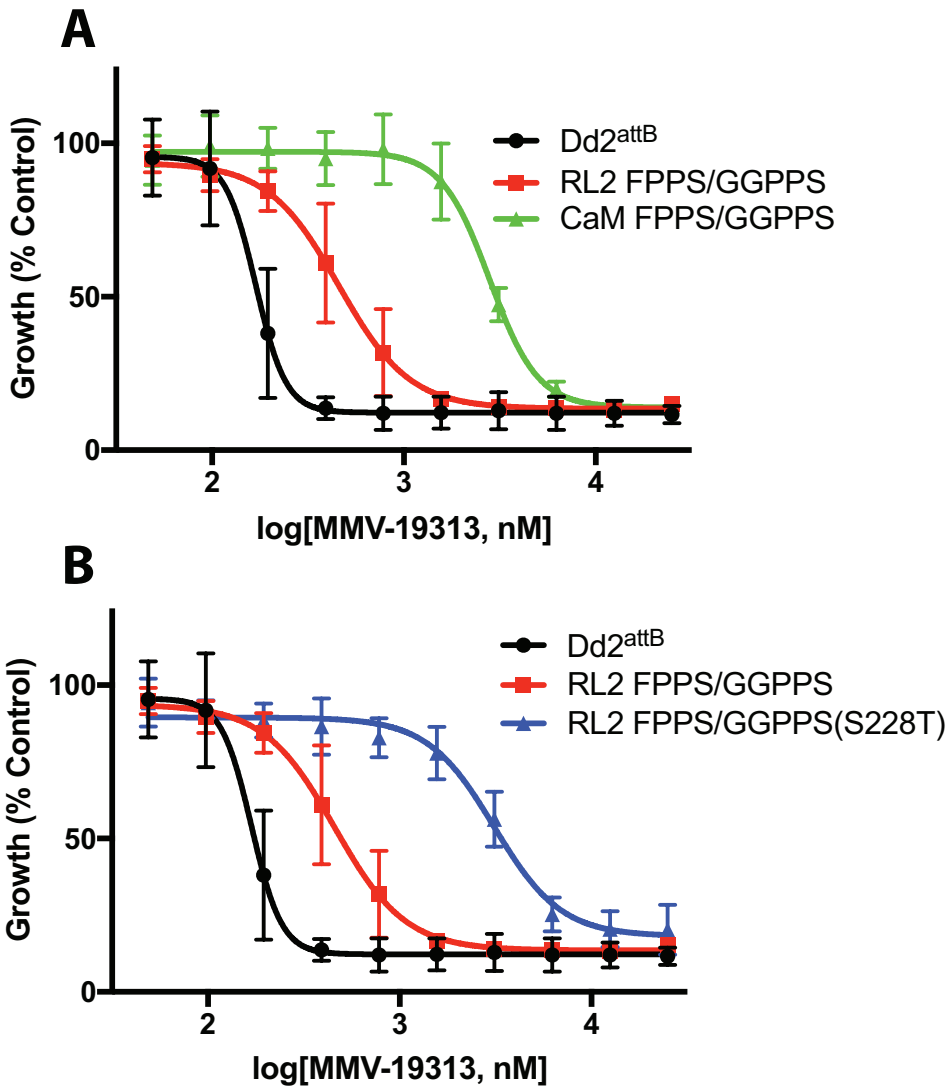

729
730 **Figure 3. Overexpression of WT and an S228T variant of *Pf*FPPS/GGPPS confer resistance**
731 **to MMV019313. A**. EC_{50} curves of MMV019313 against the parental $Dd2^{attB}$ parasites (black)
732 and parasites over-expressing FPPS/GGPPS-GFP under the RL2 (red) or CaM (green) promoter.
733 **B**. EC_{50} curves of MMV019313 against the parental $Dd2^{attB}$ parasites (black) and parasites over-
734 expressing wild type (red) or mutant (S228T, blue) FPPS/GGPPS-GFP under the RL2 promoter.
735

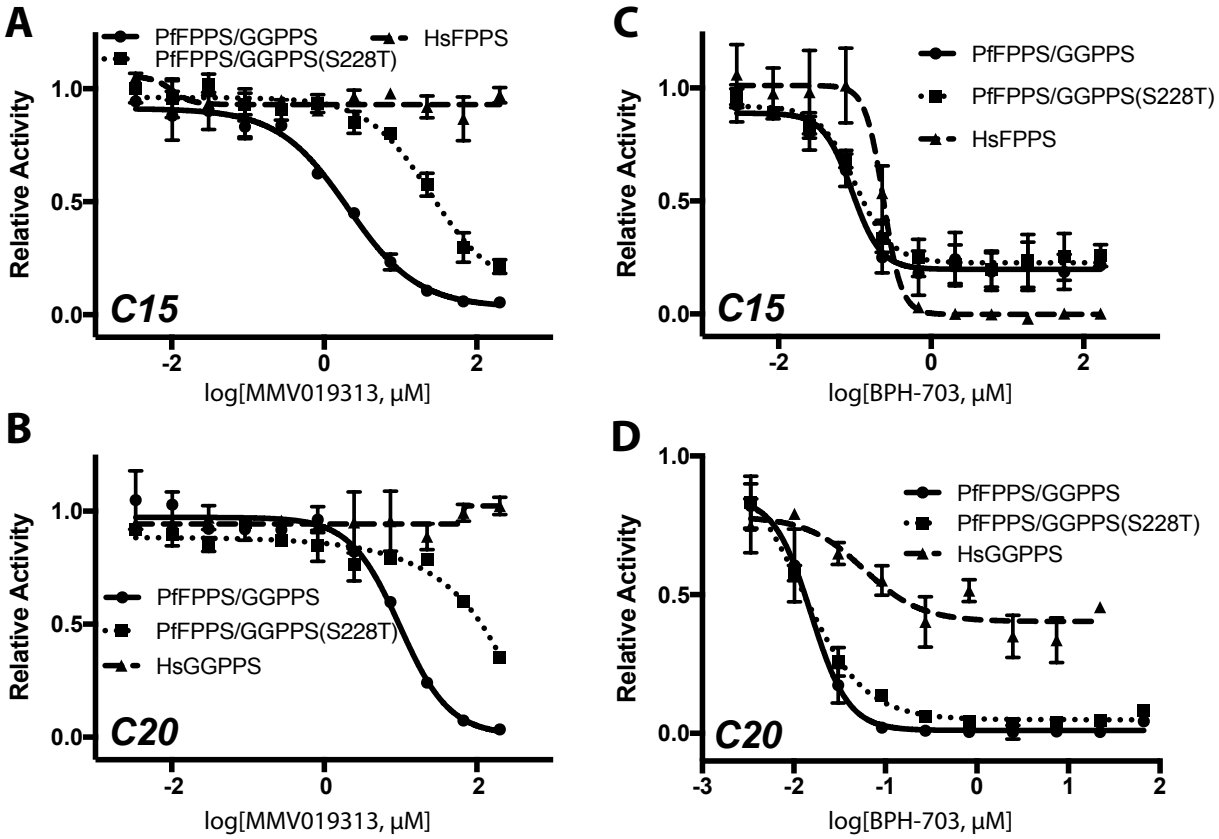

Figure 4. **MMV019313 has a specific and distinct mode-of-inhibition against purified *Pf*FPPS/GGPPS.** Dose-dependent inhibition of wild-type PfFPPS/GGPPS (solid), PfFPPS/GGPPS S228T variant (dotted), and either human FPPS or GGPPS (dashed) of **A**. FPP (C15) production by MMV019313, **B**. GGPP (C20) production by MMV010313, **C**. FPP (C15) production by BPH-703, and **D**. GGPP (C20) production by BPH-703. Partial inhibition of *Hs*GGPPS by BPH-703 was observed under k_{cat} conditions, while complete inhibition was observed under non-saturating conditions (**Figure S5**).